**Atmospheric
Chemistry
and Physics**

East Asian SO$_2$ pollution plume over Europe – Part 2: Evolution and potential impact

V. Fiedler[1,2], F. Arnold[2,1], H. Schlager[1], A. Dörnbrack[1], L. Pirjola[3,4], and A. Stohl[5]

[1]Deutsches Zentrum für Luft- und Raumfahrt, Institut für Physik der Atmosphäre, Oberpfaffenhofen, 82234 Wessling, Germany
[2]Max-Planck Institute for Nuclear Physics, (MPIK), Atmospheric Physics Division, P.O. Box 103980, 69029 Heidelberg, Germany
[3]Department of Physics, University of Helsinki, P.O. Box 64, 00014 Helsinki, Finland
[4]Department of Technology, Metropolia University of Applied Sciences, P.O. Box 4000, 00180 Helsinki, Finland
[5]Norwegian Institute for Air Research (NILU), Dept. Regional and Global Pollution Issues, Kjeller, Norway

Abstract. We report on the first observation-based case study of an aged East Asian anthropogenic SO$_2$ pollution plume over Europe. Our airborne measurements in that plume detected highly elevated SO$_2$ mole fractions (up to 900 pmol/mol) between about 5000 and 7000 m altitude. Here, we focus on investigations of the origin, dispersion, evolution, conversion, and potential impact of the observed excess SO$_2$. In particular, we investigate SO$_2$ conversion to gas-phase sulfuric acid and sulfuric acid aerosols. Our FLEXPART and LAGRANTO model simulations, along with additional trace gas measurements, suggest that the plume originated from East Asian fossil fuel combustion sources and, 8–7 days prior to its arrival over Europe, ascended over the coast region of central East Asia to 9000 m altitude, probably in a cyclonic system with an associated warm conveyor belt. During this initial plume ascent a substantial fraction of the initially available SO$_2$ must have escaped from removal by cloud processes. Hereafter, while mostly descending slowly, the plume experienced advection across the North Pacific, North America and the North Atlantic. During its upper troposphere travel, clouds were absent in and above the plume and OH-induced gas-phase conversion of SO$_2$ to gas-phase sulfuric acid (GSA) was operative, followed by GSA nucleation and condensation leading to sulfuric acid aerosol formation and growth. Our AEROFOR model simulations indicate that numerous large sulfuric

acid aerosol particles were formed, which at least temporarily, caused substantial horizontal visibility degradation, and which have the potential to act as water vapor condensation nuclei in liquid water cloud formation, already at water vapor supersaturations as low as about 0.1%. Our AEROFOR model simulations also indicate that those fossil fuel combustion generated soot particles, which have survived cloud induced removal during the initial plume ascent, have experienced extensive H$_2$SO$_4$/H$_2$O-coating, during upper troposphere plume travel. This coating may have dramatically altered the morphology and markedly increased the light absorption efficiency of soot particles.

1 Introduction

Sulfur dioxide represents a major atmospheric pollutant having direct and indirect adverse effects on air quality, climate (Seinfeld and Pandis, 2006; IPCC, 2007), and human health (e.g. Sunyer et al., 2003; Venners et al., 2003; Longo et al., 2008). Upon release to the atmosphere, SO$_2$ undergoes conversion to gaseous sulfuric acid (GSA, H$_2$SO$_4$) (e.g. Reiner and Arnold, 1993, 1994; Menon and Saxena, 1998; Fiedler et al., 2005), which strongly contributes to atmospheric acidity (e.g. Rodhe et al., 2002; Huang et al., 2008) and represents a major aerosol precursor. Due to its very low vapor pressure, sulfuric acid acts as a major precursor of secondary sulfuric acid aerosol particles (Seinfeld and Pandis, 2006), which scatter sunlight, act as very efficient water vapor condensation nuclei in water cloud formation, and act as

Correspondence to: V. Fiedler
(verena.fiedler@dlr.de)

sites of atmospheric heterogeneous chemical reactions (e.g. Ramanathan et al., 2001; Harshvardhan et al., 2002; Garrett et al., 2002; Andreae et al., 2005). Due to their large hygroscopicity, sulfuric acid aerosols undergo substantial hygroscopic size growth, which strongly increases their light scattering efficiency and ability to act as water vapor condensation nuclei in liquid water cloud formation.

Atmospheric SO$_2$ stems preferably from fossil fuel combustion and therefore is mostly anthropogenic. Uptake of sulfuric acid by fossil fuel generated soot aerosol particles dramatically alters the soot morphology, hygroscopicity, and optical properties (Fuller et al., 1999; Lesins et al., 2002; Zhang et al., 2008). Due to its indirect influence on aerosols, via GSA formation, SO$_2$ has a strong indirect influence on aerosols, clouds, the planets radiation balance, and climate (Seinfeld and Pandis, 2006; IPCC, 2007).

A very strong anthropogenic SO$_2$ source is East Asia (Lelieveld et al., 2001), particularly China, whose SO$_2$ source strength is presently increasing, due to increasing industrialization and urbanization ((Streets and Waldhoff, 2000). In 2006, the anthropogenic SO$_2$ release from China was about 31 020 gG/year (mostly due to power plants and industry) and has increased during the period 2001–2006 by a factor of 1.36 (Zhang et al., 2009). Typical SO$_2$ mole fractions in polluted regions of North China may reach up to about 20–40 nmol/mol (e.g. Thornton et al., 1997; Ding et al., 2009). Besides SO$_2$, the key precursor gas of secondary aerosols, Chinese fossil fuel combustion sources release also large amounts of primary soot aerosol particles, which are important, mostly due to their light absorption ability and light absorption induced atmospheric heating. Importantly, uptake of sulfuric acid by soot particles tends to enhance light absorption by soot particles by factors up to about 4 (Fuller et al., 1999). In 2006, the anthropogenic soot aerosol release from China was about 1811 Gg/a and had increased during the period 2001–2006 by a factor of about 1.14 (Zhang et al., 2009). Hence, in 2006, the mass ratio of anthropogenic SO$_2$ and soot released from China was about 16.

After release to the atmosphere, SO$_2$ is lost by deposition at the surface, by conversion to sulfate in water cloud droplets (Seinfeld and Pandis, 2006), and by OH-radical induced gas-phase conversion to gaseous sulfuric acid (Stockwell and Calvert, 1983; Reiner and Arnold, 1993, 1994; Lovejoy et al., 1996; Kolb et al., 1994).

Polluted planetary boundary layer air, rich in anthropogenic SO$_2$, may experience lifting to the middle and upper troposphere where SO$_2$ removal by deposition is not operative, where SO$_2$ removal by water clouds becomes less efficient, and where wind velocities are large. In these upper troposphere conditions SO$_2$ may become transported over thousands of kilometers, especially in laminar layers that cover about one fifth of the lowest 12 km of the atmosphere (Newell et al., 1999). Hence, SO$_2$ may even undergo intercontinental transport and its adverse effects may be felt far away from its sources.

The most important lifting mechanisms are deep convection, fronts, and orographic forcing. These act on different time scales ranging from hours (deep convection) to days (fronts). Outflow of East Asian anthropogenic atmospheric pollution to the Pacific, in spring, seems to occur preferably via frontal lifting over central and eastern China ahead of eastward moving cold fronts, followed by eastward transport north of 25° N (Bethan et al., 1998; Bey et al., 2001; Ding et al., 2009). Asian pollution outflow to the Pacific is strongest in spring due to frequent cyclonic activity and associated warm conveyor belts (Liu and Chan, 2003). Ahead of cold fronts, lifting of polluted planetary boundary layer air occurs within the main ascending branch of an extratropical cyclone, i.e. the warm conveyor belt (Cooper et al., 2004).

Clouds, which usually accompany lifting of planetary boundary layer air, tend to remove SO$_2$. Cloud droplets take up SO$_2$, where it may undergo chemical conversion to sulfate. This conversion depends on the cloud liquid water content, updraft velocity, droplet pH, and the availability in the droplets of SO$_2$ oxidants (particularly dissolved H$_2$O$_2$ and O$_3$), and catalysts (certain metals) (Seinfeld and Pandis, 1998). Most numerical model simulations of SO$_2$ transport in cloud systems suggest that substantial fractions of SO$_2$ may escape from scavenging by cloud processes, even in convective clouds with high liquid-water content (Barth, 1994; Kreidenweis et al., 1997; Crutzen and Lawrence, 2000). Once cloud droplets freeze, SO$_2$ uptake and conversion of still dissolved SO$_2$ ceases (Crutzen and Lawrence, 2000). As droplets freeze, still dissolved SO$_2$ will be expelled (Clegg and Abbatt, 2001) and recycled to the gasphase. Since SO$_2$ removal by water cloud processes during vertical transport is very complex, its correct representation in current global models still represents a major challenge.

By contrast to SO$_2$, the highly soluble gas-phase sulfuric acid and sulfuric acid aerosols may experience very efficient removal by cloud processes. Therefore, after transport of a fossil fuel combustion plume through the precipitation formation region of an active cyclone, one may expect, in the very early outflow of the cyclonic system, low concentrations of sulfate aerosols but appreciable mole fractions of SO$_2$ and large mole fractions of NO$_y$ (mostly peroxyacetylnitrate). Support for this view was previously obtained from airborne measurements of SO$_2$ made over North East China in the early outflow of a cyclone (Ding et al., 2009). At an altitude of about 2600 m, close to the border of China and North Korea,, SO$_2$ mole fractions of up to 14.6 nmol/mol were detected.

During long-range transport in the middle and upper troposphere, SO$_2$ undergoes OH-induced gas-phase conversion to GSA and dilution due to plume dilution caused by entrainment of ambient air. Since water clouds are frequently absent in the middle and upper troposphere, SO$_2$ removal by water cloud processes is reduced and OH-induced SO$_2$ conversion is enhanced and may be even more enhanced due to enhanced OH formation resulting from UV-backscattering
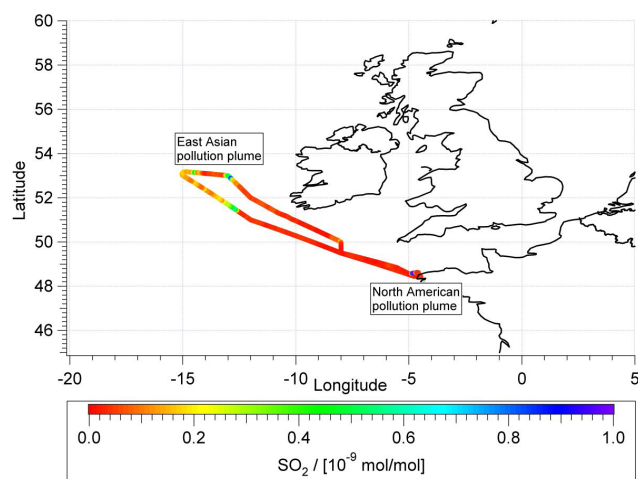
Fig. 1. Falcon flight path on 3 May 2006, color coded with the measured SO$_2$ mole fraction.

Fig. 2. Time series of the SO$_2$ mole fraction of the INTEX-B flight on 3 May 2006, smoothed with a running mean averaging 30 data points which corresponds to a time resolution of 30 s. Also plotted is the flight altitude.

by underlying low altitude clouds. In spring, the upper troposphere SO$_2$ lifetime with respect to reaction with OH is of the order of 10–20 days (Finlayson-Pitts and Pitts, 2000).

Previously, intercontinental transport of anthropogenic SO$_2$ has been observed, particularly transport from East Asian SO$_2$ sources to the Pacific and North America and from North American SO$_2$ sources to the Atlantic and Europe. For example, Arnold et al. (1997) observed a strong North American SO$_2$ plume over Europe, whose maximum SO$_2$ mole fraction was about 3000 pmol/mol. Brock et al. (2004) reported observations of East Asian SO$_2$ over the North Pacific and off the west coast of North America. However, to our knowledge, observations of very long-range SO$_2$ transport from East Asian sources across the Pacific, North America, and the Atlantic to Europe have so far not been reported.

The model simulations in this paper are performed with an atmospheric chemistry and aerosol dynamics model AERO-FOR (Pirjola, 1999; Pirjola and Kulmala, 2001). Previous similar model simulations have been published e.g. by Pirjola et al. (1999) and by Laaksonen et al. (2000).

Previous measurements and modeling of particle formation in the upper troposphere have also been reported by Lee et al. (2003, 2004). They found that cirrus clouds provide favorable conditions for particle formation, but their model results considered ion induced nucleation and are therefore not directly comparable to ours.

In the present paper, we report on investigations of the origin, evolution, and effects of such an East Asian SO$_2$ plume, which we have probed over Europe by airborne instruments. The measurements and experimental details can be found in the accompanying paper by Fiedler et al. (2009), hereafter termed paper A.
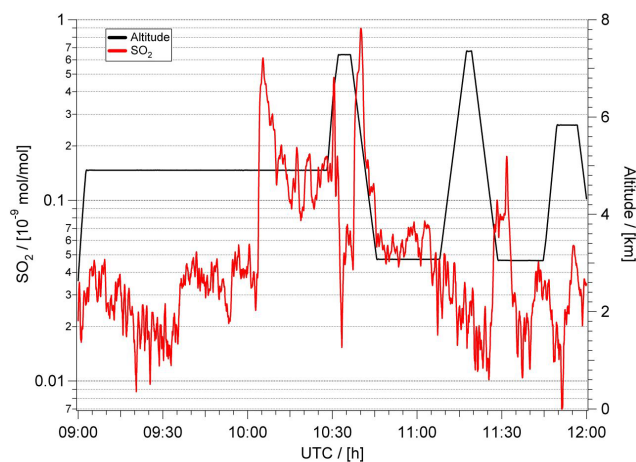
2 Plume measurements

The experimental aspects of our East Asian SO$_2$ plume observations over Europe will only briefly be reviewed here. The airborne SO$_2$ measurements were made by an advanced CIMS instrument (CIMS = Chemical Ionization Mass Spectrometry) aboard the German research aircraft Falcon and took place on 3 May 2006 over the Atlantic, about 200 km west of Ireland. Our measurements were an integral part of the second phase of the International Chemical Transport Experiment–Phase B (hereafter termed INTEX B) campaign, which took place from 17 April to 15 May 2006 and included measurements over the Pacific, North America, and the Atlantic (see overview paper by Singh et al., 2009).

Our advanced CIMS instrument was equipped with an ion trap mass spectrometer and was permanently calibrated in flight. It offered a high sensitivity, a high time resolution (time response as good as 0.1 s) and translates to a high spatial resolution (see paper A). The objective of the 3 May 2006 Falcon flight was to intercept and probe an East Asian pollution plume, which had been predicted by FLEXPART lagrangian particle dispersion model simulations (Stohl et al., 2002, 2005) (see below) to be present on 3 May over the East Atlantic and the British isles. The focus of our measurements was on SO$_2$, the key precursor of East Asian secondary aerosols.

Figure 1 shows the flight path of the Falcon along with color coded measured SO$_2$ mole fractions. In the region about 200 km west of Ireland, where the predicted East Asian plume was expected, increased SO$_2$ mole fractions of up to 900 pmol/mol were observed.

Figure 2 shows a time sequence of the measured atmospheric SO$_2$ mole fractions along with the Falcon flight
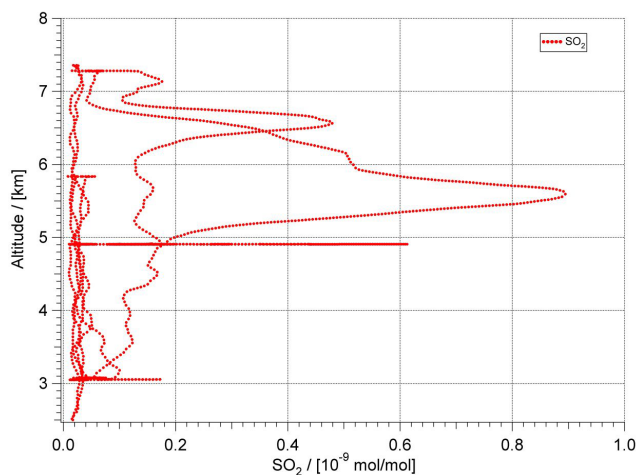
Fig. 3. Vertical distribution of SO$_2$ mole fractions measured above 2300 m on the Falcon flight of 3 May 2006.

altitude. As the Falcon was cruising at 4900 m, it entered the plume as indicated by a sudden steep increase of SO$_2$ from 40 to 600 pmol/mol. As the Falcon continued its cruise at the same altitude, SO$_2$ decreased to about 140 pmol/mol and as the Falcon ascended to 7400 m, it penetrated an SO$_2$-rich (500 pmol/mol) stratified plume located at about 6600 m. As the Falcon descended again to 3000 m, it penetrated an SO$_2$-rich (900 pmol/mol) stratified plume at 5600 m.

Figure 3 shows the vertical distribution of SO$_2$ mole fractions measured above 2300 m. Stratified SO$_2$-rich plumes are clearly noticeable, particularly between about 4000 and 7000 m altitude. The data reveal that the spatial SO$_2$ distribution is highly inhomogeneous, both vertically and horizontally.

Besides SO$_2$, gaseous NO$_y$ (sum of reactive nitrogen gases: mostly HNO$_3$ and peroxyacetylnitrate) was also enhanced in the plume and the molar ratio of excess SO$_2$ and excess NO$_y$ was about 1.4. Fossil fuel combustion sources release, besides SO$_2$, also large amounts of NO$_y$, preferably as NO$_x$ (mostly NO and NO$_2$) and the molar emission ratio for SO$_2$ and NO$_y$ is typically about 1–4. After release, NO$_x$ experiences conversion to HNO$_3$ and PAN (peroxyacetylnitrate). Since HNO$_3$ is highly soluble in liquid water, it may undergo efficient liquid cloud induced removal. This may have occurred during the initial ascent but not during the upper troposphere travel of the plume parcel (see below). By contrast, PAN is not soluble in liquid water and therefore should not be affected appreciably by cloud-induced removal. In fact, measurements of NO$_y$, PAN, NO$_x$, and HNO$_3$ made during INTEX B in aged (7–10 days) East Asian pollution plumes over the East Pacific (Dunlea et al., 2008) observed NO$_y$ mole fractions of about 500 pmol/mol and found that NO$_y$ is mostly PAN. As will be shown below, on a time scale of 8 days, about half of the SO$_2$ experiences conver-

sion to GSA during free troposphere transport. Hence after 8 days, the molar ratio SO$_2$/NO$_y$ may be similar to the corresponding molar emission ratio.

Our measured molar ratio SO$_2$/NO$_y$ of 1.4 is in fact similar to the expected molar emission ratio (1–4) for fossil fuel combustion, but much larger than the corresponding molar emission ratio for bio mass burning (<0.1) and much smaller than the molar emission ratio for Ni-Cu smelting industry sources (about 40). Hence, the above measured SO$_2$/NO$_y$ ratio of 1.4 suggests that fossil fuel combustion was the major source of the observed excess SO$_2$ and excess NO$_y$ (see also paper A).

3 Plume transport and dispersion

To investigate the evolution (trajectory, age, dispersion, and dilution) of the observed SO$_2$-rich air parcel, we have made model simulations using the FLEXPART (Stohl et al., 2002, 2005) and LAGRANTO (Wernli and Davies, 1997) models (see also supplementary material http://www.atmos-chem-phys.net/9/4729/2009/acp-9-4729-2009-supplement.zip). The back-trajectory simulations (see Fig. 1 in the supplementary material) suggest that, on 23 April, 10 days prior to our measurements, the air parcel of interest passed at altitudes of about 2000 m over central East Asia. There, the air parcel has probably taken up large amounts of anthropogenic SO$_2$. The location of SO$_2$ sources and their individual relative contributions to the "inert SO$_2$" tracer, as simulated by FLEXPART, have been thoroughly discussed in part 1 of the paper (Fiedler et al., 2009). Hereafter, on 24–25 April, the SO$_2$-rich air parcel (hereafter termed plume parcel) ascended to about 9000 m altitude, probably in a cyclonic system with an associated warm conveyor belt (see movie 1 in the supplementary material: http://www.atmos-chem-phys.net/9/4729/2009/acp-9-4729-2009-supplement.zip). However, considering the plume parcel age, the FLEXPART simulations and therefore the above picture of the plume parcel origin and history have marked uncertainties. This should be born in mind for the entire following discussion.

To investigate the plume parcel dispersion we have also made forward simulations using the FLEXPART model. Figure 4 shows forward simulations for four selected days. Given is the distribution of an inert tracer released from surface SO$_2$ sources located in East Asia (see figure in supplementary information: http://www.atmos-chem-phys.net/9/4729/2009/acp-9-4729-2009-supplement.zip). Plotted is the vertical mass column at 12:00 UTC for the days 26 April, 1 May, 2 May and 3 May 2006. A movie with a higher (12 h) time resolution can be found in the supplementary information. The forward simulation started already on 20 February 2006 to include also earlier emissions. For each day, the approximate position of the plume parcel (as inferred from the back-trajectory) intercepted by the Falcon on 3 May is
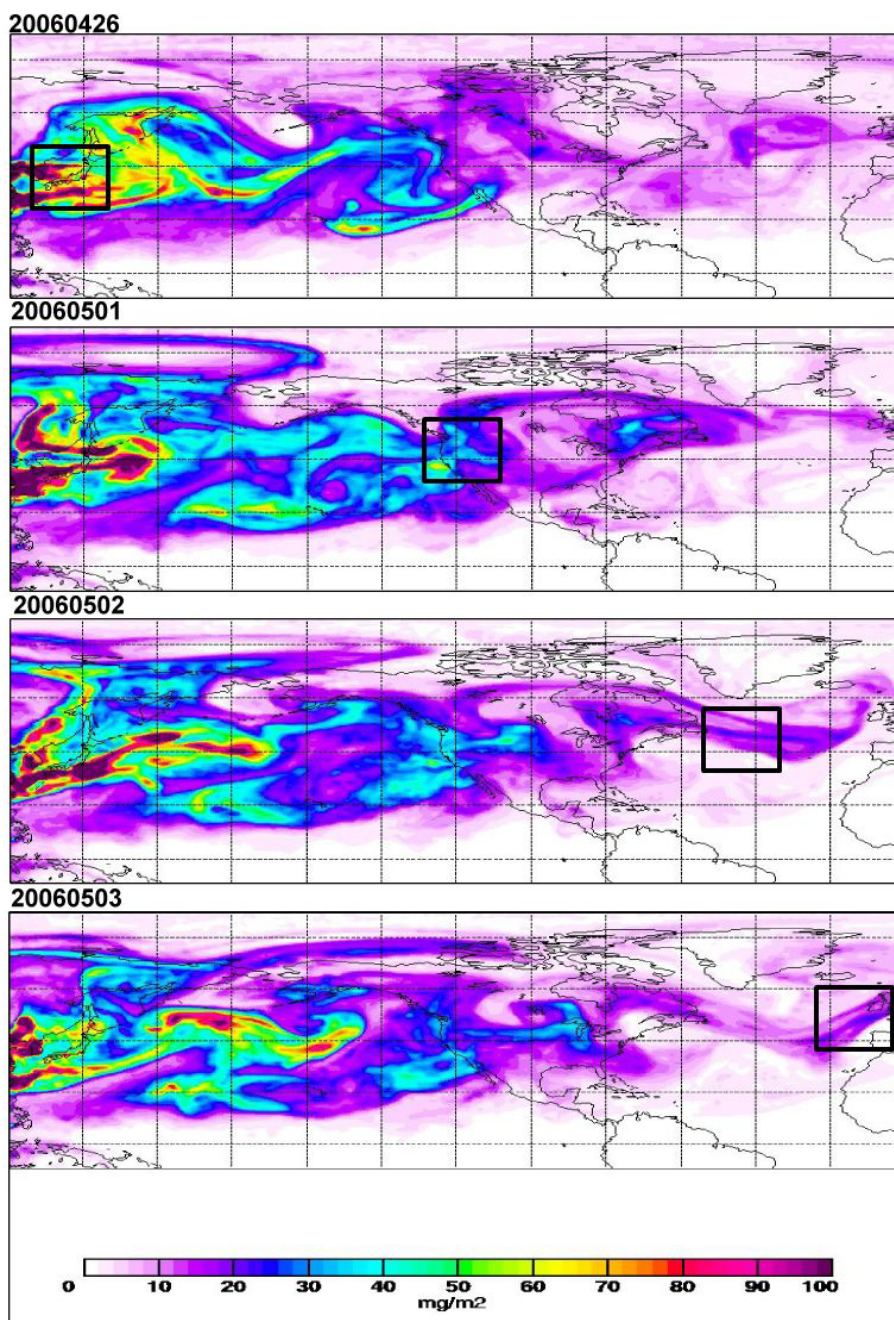
Fig. 4. FLEXPART forward simulations of East Asian SO$_2$ (neglecting SO$_2$ removal processes) for the days 26 April 2006 and 1–3 May 2006. Plotted is the vertical mass-column at 12:00 UTC. A movie with a 12 h time resolution can be found in the supplementary information (http://www.atmos-chem-phys.net/9/4729/2009/acp-9-4729-2009-supplement.zip).

indicated by a box. The inert tracer experienced preferably eastward transport across the North Pacific, North America, and the North Atlantic. During transport, the plume experienced substantial dilution due to mixing with ambient air. On 26 April, the day after the initial ascent, tracer columns are about 100 mg/m^2. Above the central North Pacific, plume filaments with still large tracer columns ($>$50 mg/m^2) are present. Above North America, columns are mostly below 40 mg/m^2. Above the North Atlantic columns are below 25 mg/m^2, and in the region where the Falcon measurements of 3 May took place, columns are about 10–20 mg/m^2. This implies a dilution of the probed plume parcel by a factor of about 5 to 10.
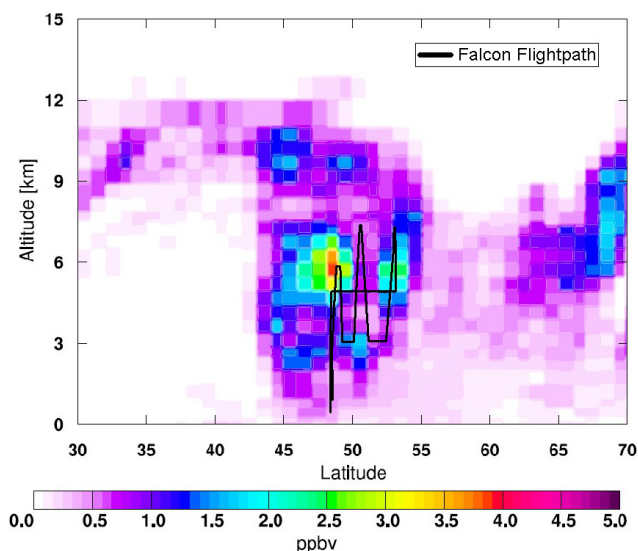
Fig. 5. FLEXPART vertical distribution of the SO$_2$ mole fraction at 12.5 degrees Longitude (mean value on 3 May 2006 from 09:00 to 12:00 UTC, ppbv = parts per billion by volume=nmol/mol). Only SO$_2$ is considered which has been released from Chinese sources. SO$_2$ removal has been neglected. Also given is the vertical footprint of the Falcon flight path (black line).

Figure 5 shows an altitude-latitude cross section of the predicted inert plume tracer mole fraction (for a longitude of 12.5 degrees West). Indicated is the flight path of the Falcon. The core of the predicted plume extends from about 5000 m–7000 m, which is consistent with the observed SO$_2$ plume (Fig. 3) extending also from about 5000–7000 m. Hence, the FLEXPART forward simulations of the inert tracer reproduce approximately the horizontal and vertical distribution of the plume. The modeled "inert SO$_2$" mole fractions, in that part of the plume core are about 2.5–4 nmol/mol. Hence, about 22–36% of the predicted "inert SO$_2$" were actually observed. If the plume parcel dilution was correctly reproduced by the simulation, the missing SO$_2$ (64–78%) must have been lost by reaction with OH during the upper tropospheric plume parcel travel (see below) and by cloud processes during the initial ascent.

During the upper troposphere travel of the plume parcel, clouds were absent inside and above the plume parcel. This is demonstrated by Figs. 6 and 7.

Figure 6 shows MODIS satellite images of cloud-top pressures (Xiong et al., 2009; Menzel et al., 2008). The figure is composed of 8 individual panels, corresponding to the 8 days of the period 26 April to 3 May 2006. Indicated by dots (separated by 6 h) is the LAGRANTO back-trajectory of the air mass of interest. The trajectory was obtained by the LAGRANTO model by consideration of ECMWF meteorological data. The color of the dots indicates the pressure of the air mass (see also Fig. 7).

Figure 7 (upper panel) shows a time-sequence of pressures in the plume (prepared by a meteorological analysis using ECMWF data and the LAGRANTO model) along with lowest cloud-top pressures (taken from Fig. 6) for each day. On 23–24 April, the minimum cloud-top pressure was always similar to the plume pressure, which indicates that clouds were present in the plume. Hereafter, it was mostly higher than the plume pressure with exception of short time intervals when it became similar to the cloud top pressure. Figure 7 (lower panel) shows meteorological data for the plume intercepted by the Falcon on 3 May 2006. The data were prepared using ECMWF data and the LAGRANTO model. Plotted are temperature, and relative humidities with respect to liquid water (RHW) and water ice (RHI) and the water vapor mass mixing ratio. Also given is the plume altitude.

From the preceding discussion the following, admittedly uncertain, picture of the SO$_2$ evolution in the plume parcel emerges: On 23 April the plume passed at relatively low altitudes (around 2000 m) over heavily polluted central East Asia, where it has taken up SO$_2$, released from anthropogenic fossil fuel combustion sources. On 24–25 April the plume ascended to about 7800 m. During the ascent, maximum RHW=68% and RHI=102% were reached at 3600 m where the temperature was 266 K. As the plume ascended further, temperature was still decreasing but RHW decreased steeply again whereas RHI remained almost constant. On 25 April at 00:00 UTC, while the plume was further ascending to 9000 m, also RHI started to decrease. The plume ascent of 24–25 April was most likely due to a cyclonic system with an associated warm conveyor belt. Satellite cloud images indicate the presence of a cyclonic system (see movie in the supplementary information: http://www.atmos-chem-phys.net/9/4729/2009/acp-9-4729-2009-supplement.zip). It seems that during the ascent of 24–25 April a large fraction of the SO$_2$ escaped from scavenging by cloud processes. This is consistent with previous investigations, which suggested that ascent of a pollution plume in a warm conveyor belt may remove relatively little SO$_2$ but a large fraction of aerosols (Arnold et al., 1997; Brock et al., 2004; Ding et al., 2009).

Figure 7 suggests that, on 24 April, liquid water clouds formed in the plume parcel, followed by cloud droplet freezing and the presence of ice clouds, which persisted also during the first half of 25 April. During late 25 April and during 26 April, the plume parcel descended rapidly to about 6000 m, T increased to 235 K, and RHW and RHI decreased to less than 30%. On the following 3 days (27–29 April), the descent of the plume parcel continued to about 5400 m and RHW and RHI remained below 30%. On 30 April and 1 May the plume parcel ascended from about 5400 to 7500 m and RHW and RHI increased to 58% and 86%, respectively. On early 1 May, cloud-top pressures are close to plume parcel pressures (Figs. 6 and 7). Hence, on 1 May, an ice cloud may have been present for a few hours in the plume parcel. Already in the morning of 1 May, the plume parcel descended again to about 5000 m. On 3 May, the
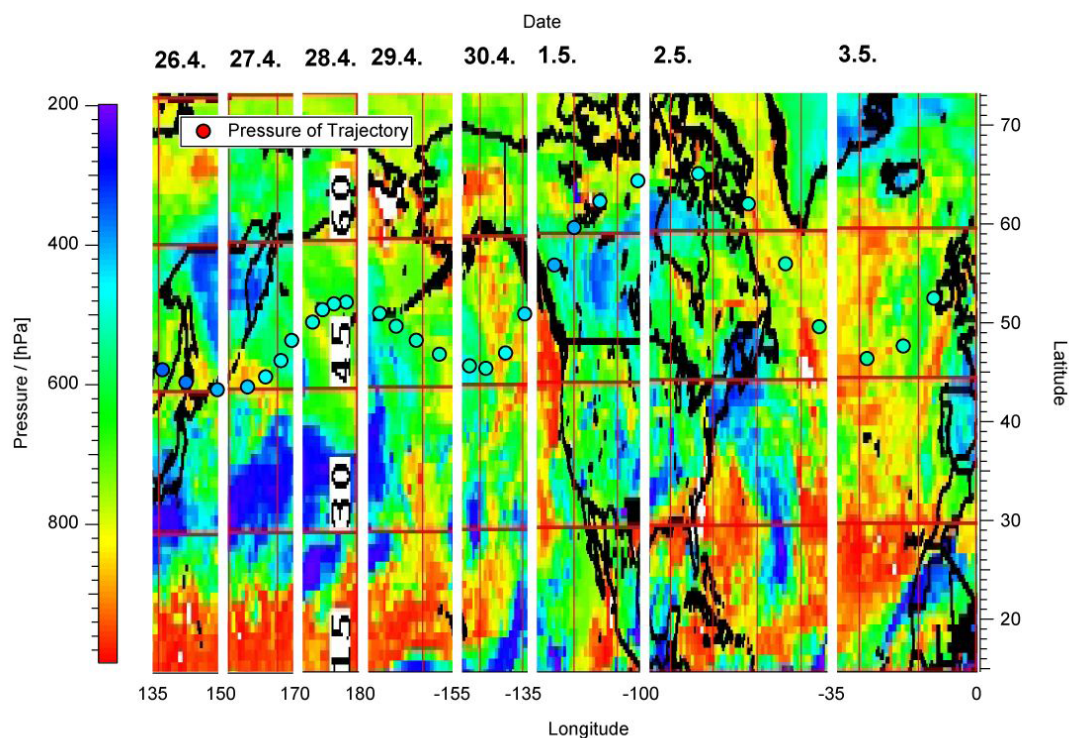
Fig. 6. MODIS satellite cloud top pressures. The figure is composed of 8 panels corresponding to the days from 26 April 2006 to 3 May 2006. Indicated by dots (separated by 6 h) is the trajectory of the air mass of interest. The trajectory was obtained by the LAGRANTO model by consideration of ECMWF meteorological data. The color code gives the cloud top pressure and also the pressure of the plume parcel trajectory, see also Fig. 7.

plume parcel ascended where it was intercepted by the Falcon, preferably between 10:00 and 10:45 UTC and at altitudes between 5000 and 7000 m. On 29 and 30 April when cloud-top pressures were similar to plume parcel pressures (Fig. 7), the RHI were always below 30%, which does not allow the presence of clouds in the plume. The meteorological data of Fig. 7 suggest that liquid water clouds were not present in the plume parcel during the entire period 26 April to 3 May. Therefore, significant cloud induced removal of SO$_2$ and H$_2$SO$_4$/H$_2$O aerosols should not have occurred during that period.

4 Conversion of SO$_2$

Using the AEROFOR model, we have simulated SO$_2$ conversion to gas-phase sulfuric acid (GSA), followed by GSA conversion to sulfuric acid aerosols. This simulation is restricted to the period 26 April–3 May when clouds were absent inside and above the plume parcel. AEROFOR (e.g. Pirjola, 1999; Pirjola and Kulmala, 2001) is a Lagrangian type sectional box model used to investigate the formation and growth of particles under clear sky atmospheric conditions. The model includes the gas-phase chemistry and aerosol dynamics, and calculates the number size distribution of particles as a func-

tion of time. The meteorological data – six hourly values of pressure, temperature and water vapor concentration – are obtained from the trajectory. The processes that are included in the model in this work are: 1) chemical production of OH and H$_2$SO$_4$ in the gas phase, 2) homogeneous binary H$_2$SO$_4$-H$_2$O nucleation (Vehkamäki et al., 2002), 3) condensation of H$_2$SO$_4$ and H$_2$O (Fuchs and Sutugin, 1971), 4) inter- and intramode coagulation of particles (Fuchs, 1964), 5) dilution by entrainment with free troposphere and 6) concentration corrections (ideal gas law) due to pressure and temperature variations. It should be noted that since the model is running under clear sky conditions, cloud processing, coalescence and wet deposition are not taken into account.

Preexisting particles present in the air mass after the initial ascent are not known and difficult to model and therefore were prescribed in the model simulations. Different model runs (A, B, C, D, E) have been made assuming different preexisting particle concentrations. Run A assumes that preexisting particles were absent due to complete cloud induced particle scavenging during the initial ascent. Runs B, C, D and E assume bimodal size distribution to the preexisting particles with the total number concentration of 250, 500, 1000 and 2000 cm^{-3}, respectively. The preexisting Aitken mode possesses lognormal parameters of N_{ait}=200, 400, 800 and
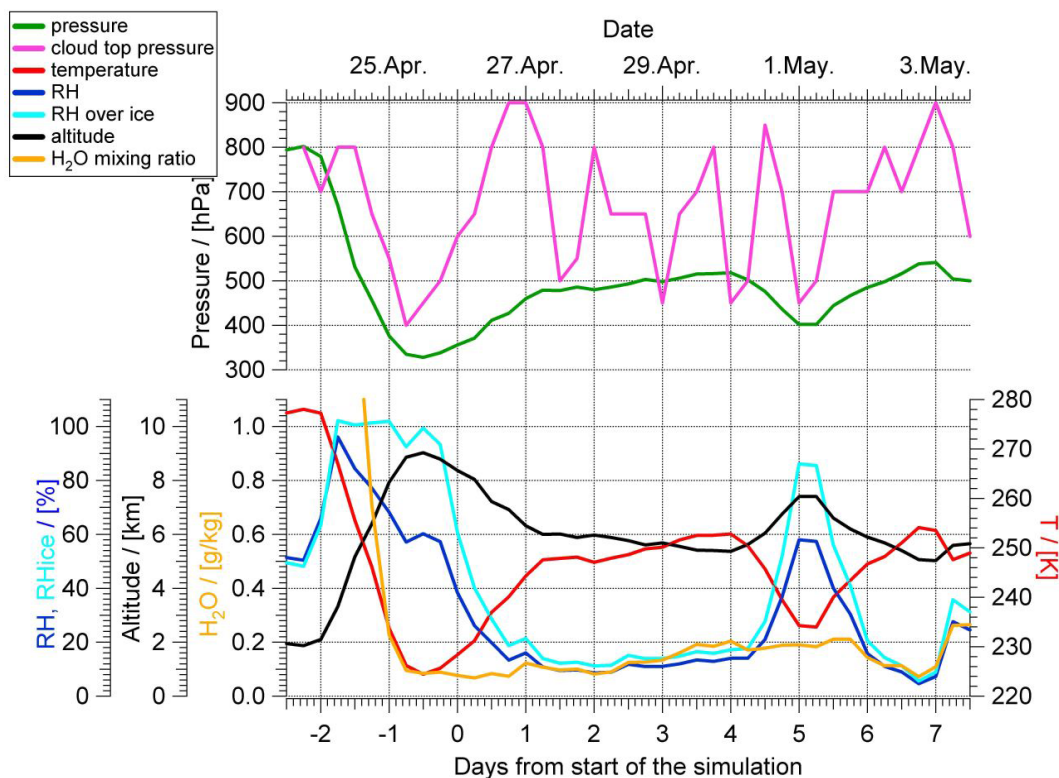
Fig. 7. Upper panel: Pressure of the plume parcel trajectory during transport from Asia to Europe as well as cloud top pressures. Lower panel: meteorological data (temperature, RH, RH over ice, altitude, H$_2$O mass mixing ratio) for the plume derived from ECMWF data by use of the LAGRANTO model.

Table 1. Number concentrations of initial particles N$_1$ (60 nm diameter) and N$_2$ (180 nm diameter) in the five model cases A–E. The initial SO$_2$ concentration was in all cases the same.

Model Case	A	B	C	D	E
Initial Particles N$_1$ [cm^{-3}]	0	200	400	800	1600
Initial Particles N$_2$ [cm^{-3}]	0	50	100	200	400
Initial SO$_2$ concentration [cm^{-3}]			2.9×10^{11}		

1600 cm^{-3} (respectively) with the geometric mean dry diameter of d_{ait}=60 nm and standard deviation of σ_{ait}=1.45; and the preexisting accumulation mode N_{acc}=50, 100, 200 and 400 cm^{-3} (respectively), with d_{acc}=180 nm (dry diameter) and σ_{acc}=1.9. The assumed preexisting mode sizes are in agreement with the measurements by de Reus et al. (2001). Table 1 summarizes the initial particle concentrations of the five model cases. The initial SO$_2$ concentration was inferred from the SO$_2$ measured on 3 May by consideration of SO$_2$ depletion by plume dilution and SO$_2$ reaction with OH. The initial value was then 2.9×10^{11} cm^{-3}.

The total (due to horizontal plus vertical mixing) plume dilution ratio during that period was considered to be 5 or 10

(base model runs), as indicated by the FLEXPART forward simulations. The lognormal parameters to the size distribution of the ambient free tropospheric particles entrained with the box were adopted from Raes et al. (1997); N=425 cm^{-3}, d=53 nm (dry diameter), σ=1.9. The free tropospheric SO$_2$ concentration was assumed to be 40 pmol/mol. Sensitivity tests have been made for different plume dilution ratios, OH concentrations, and nucleation rates.

After its initial ascent of 24–25 April, when clouds were absent in and above the plume parcel, solar UV-radiation induced OH formation took place in the plume parcel, followed by OH-induced conversion of SO$_2$ to gaseous sulfuric acid. Since underlying clouds were often present, the UV-radiation in the air mass was often enhanced due to UV-backscattering by the underlying clouds which increased the rate of OH-induced gaseous sulfuric acid (GSA) formation by up to a factor of 2. In a first simulation step the OH concentration was calculated considering O$_3$, H$_2$O, solar elevation dependant UV-radiation, and effects on UV-radiation by clouds. In a second step the calculated OH and the reconstructed SO$_2$ (reconstructed by consideration of SO$_2$ depletion by plume dilution and SO$_2$ reaction with OH) were used to calculate the rate of GSA formation.
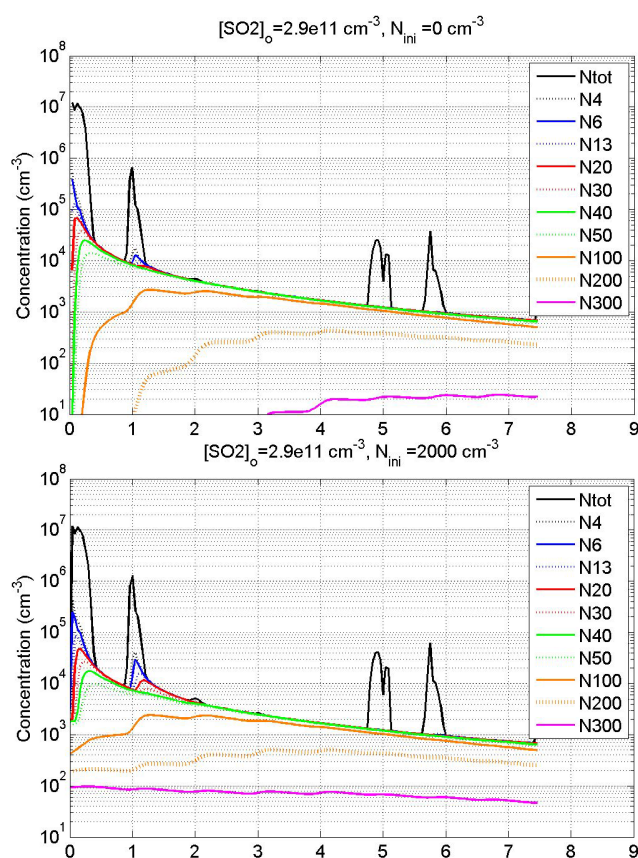
The time sequence of the AEROFOR modeled concentrations of OH and SO$_2$, the rate of GSA formation, GSA concentration, the binary nucleation rate and the condensation sink (CS, this is the inverse GSA lifetime) are shown in figures included in the supplementary information (http://www.atmos-chem-phys.net/9/4729/2009/acp-9-4729-2009-supplement.zip). These results are results of run A and E.

The OH concentration (Fig. 3 in the supplementary information) exhibits a characteristic secant-like daytime diurnal variation with maximum number concentrations of about 3×10^6 cm^{-3}, which implies a 1/e-lifetime of SO$_2$ of about 10 days. Therefore, during the 8 day upper troposphere travel of the plume, the reaction of SO$_2$ with OH removes about half of the SO$_2$. Hence, without SO$_2$ loss by reaction with OH during the upper troposphere travel, the SO$_2$ in the plume parcel, on 3 May, would not have been 0.9 nmol/mol (as measured) but 1.8 nmol/mol. If so, the missing SO$_2$ would have been only about 0.7–2.2 nmol/mol. If FLEXPART correctly reproduces plume dilution and AEROFOR correctly reproduces OH-induced SO$_2$ loss, this missing SO$_2$ must have been removed by cloud processes during the initial ascent. For total plume dilution factors of 5–10 (see above), the SO$_2$ just after the end of the liquid water cloud phase of the initial ascent (at about 3400 m altitude; see Fig. 7) would have been about 9–18 nmol/mol. In comparison, the SO$_2$ measured by Ding et al. (2009) at 2600 m above North East China in the very early outflow of a cyclonic system of 14.6 nmol/mol falls in between our above range of 9–18 nmol/mol. The sulfate measured during INTEX B in aged (7–10 days) East Asian pollution plumes over the East Pacific (see Dunlea et al., 2008) was about 3 μg/sm^3 (sm^3 means m^3 at standard conditions). In comparison, the sulfate expected to be present in the plume parcel (on 3 May; plume parcel age: about 8 days) which we have probed on 3 May, is similar up to about 3.6 μg/sm^3.

A simulation of SO$_2$ removal by cloud processes during the initial ascent is complex and very uncertain and therefore is beyond the scope of the present paper.

The GSA formation rate calculated from the modeled OH and SO$_2$ is shown in Fig. 4 of the supplementary information. It exhibits a diurnal variation with maximum noontime values, which decrease from about 2×10^6 cm^{-3} s^{-1} to 8×10^4 cm^{-3} s^{-1} during the AEROFOR simulation period (26 April–3 May). This steep decrease reflects mostly the steep decrease of the SO$_2$ concentration.

The GSA concentration (Fig. 3 of the supplementary information: http://www.atmos-chem-phys.net/9/4729/2009/acp-9-4729-2009-supplement.zip), is determined by a near steady state of GSA formation and GSA loss by conversion to aerosols and exhibits a diurnal variation with noontime maxima of about 2.5×10^7–8×10^7 cm^{-3}. The GSA concentration is much less variable than the GSA production since the steep decrease of the GSA production is approximately compensated by a strong increase of the GSA lifetime (1/CS).


Fig. 8. AEROFOR model results for aerosol particles (run A, upper panel and run E, lower panel). Plotted is a time sequence of the number concentrations Nd of sulfuric acid aerosol particles with dry diameters larger than d (in nm). Also shown is the total number concentration Ntot of sulfuric acid aerosol particles.

5 Sulfuric acid aerosol formation and growth

The binary H$_2$SO$_4$/H$_2$O nucleation rate J (see Fig. 2 of the supplementary information: http://www.atmos-chem-phys.net/9/4729/2009/acp-9-4729-2009-supplement.zip) is large $(1.5 \times 10^5$ cm^{-3} s$^{-1})$ on the first day of the simulation. Hereafter only 3 relatively weak nucleation events occur. Hence, new particle formation in the plume took place preferably on 26 April, the first day after the initial ascent.

The condensation sink CS (inverse GSA lifetime with respect to condensation on aerosols) was calculated from the size distribution of simulated aerosol particles. Although in this model run (run A) preexisting aerosols are absent, CS becomes on 26 April very large (0.032 corresponding to a GSA lifetime of only about 31 s) since J is large and numerous new particles are present, which scavenge GSA. The GSA concentration exhibits a diurnal variation, which reflects the diurnal variation of the GSA precursor OH. Diurnal GSA maximum concentrations are up to about 8×10^7 cm^{-3}. GSA is decreasing during the simulation period, but not as strongly
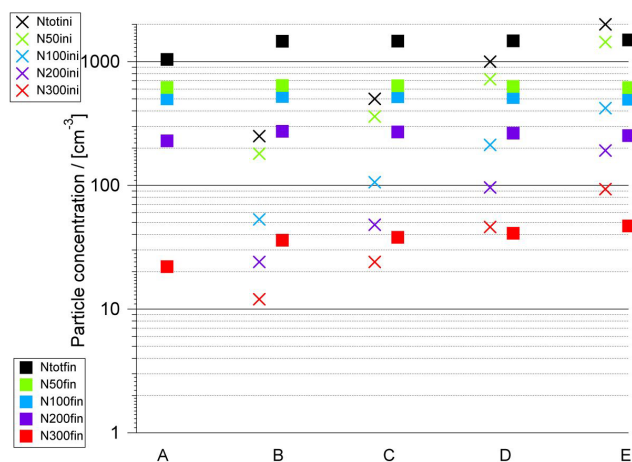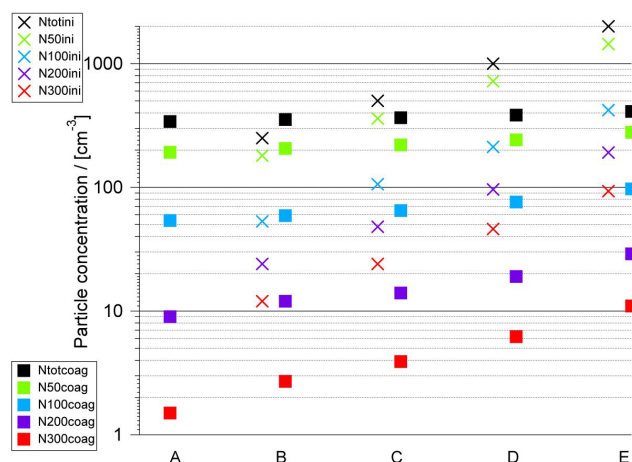
Fig. 9. Final and initial aerosol number concentrations (Ntot, N50, N100, N200 and N300) in the plume parcel obtained from the AEROFOR model (runs A, B, C, D and E).

Fig. 10. Same as Fig. 9, but without sulfuric acid formation.

as SO₂ since the GSA lifetime increases due to particle dilution and coagulation (see below).

Figure 8 (upper panel) shows AEROFOR model results for aerosol particles (run A). All times are in UTC and the particle classification to Ni (particles whose diameter is larger than i nm) is based on particle dry diameter. The total aerosol number concentration Ntot is large on 26 April reaching up to about 1×10^7 cm^{-3}. As solar elevation decreases in the afternoon and therefore OH and GSA decrease, Ntot decreases rapidly preferably due to mutual coagulation of newly formed particles and also due to plume dilution. After 26 April, when J is not large anymore, Ntot decreases almost monotonously due to coagulation and plume dilution and, on 3 May at the time of our measurements, is about 1040 cm^{-3}. Compared to Ntot, concentrations of large particles reach their maxima at later times. For example N200 reaches its maximum of 430 cm^{-3} only on 30 April. At the time of the measurements N200 is still 230 cm^{-3}. N300 reaches its maximum of 24 cm^{-3} on 2 May. Already on 30 April N100 is approximately equal to Ntot, which implies that almost all particles have dry diameters larger than 100 nm.

Figure 8 (lower panel) shows the same as Fig. 8 (upper panel), but for the AEROFOR model run E (Ni=2000 cm^{-3}). Now, values for Ntot are slightly higher on nucleation days compared to run A, but the final value on 3 May stays nearly the same. Initial and final particle concentration values can be easier compared in the following figures.

Figure 9 shows for model runs A, B, C, D and E final and initial Ntot, N50, N100, N200, and N300. For example, final N200 are about 270 cm^{-3} and nearly the same for all model runs. Final N300 are about 20–40 cm^{-3} and markedly exceed initial N300 besides for runs D and E. For run E, the final N300 is markedly smaller than the initial N300. Figure 10 shows the same as Fig. 9 but now GSA formation

and therefore GSA induced particle formation and growth are switched off. Now particle growth is only due to coagulation. Final N200 exceed initial N200 only for run A. By contrast, for the other runs, final N200 become increasingly smaller than initial N200. When comparing Figs. 9 and 10, final Ntot, N50, N100, N200, and N300 are much larger for Fig. 9. Obviously sulfuric acid formation leads to strong particle growth, which tends to strongly increase particle concentrations. This compensates the influence of plume dilution, which tends to strongly decrease particle number concentrations.

The following sensitivity studies were made. The simulation of model case C was repeated to test the response of the CCN concentration after 7.5 days to variations of the initial SO₂ concentration, OH concentration, nucleation rate, and dilution. Since the classical binary nucleation theory seems to overestimate nucleation rates in the free troposphere (Vehkamäki et al., 2002) compared to the observations (e.g. Hanson and Lovejoy, 2006), the nucleation rate was divided by a factor of 100. The final N50, N100, N200 and N300 decreased only by ≈3%. As mentioned above, the trajectory was often above the cloud tops leading to an approximately doubled OH concentration. When doubling OH, the nucleation rate increased by a factor of about 2 and also the growth of particles increased. Consequently, the final N100 increased by about 4% whereas N200 increased by 26% and N300 even by 76%. When multiplying the initial SO₂ by a factor of 2 (the final SO₂ was 3.4×10^{10} cm^{-3} which corresponds to 2300 pmol/mol), the final N200 and N300 increased by 26% and 240%, respectively. Obviously the formation of particles is more sensitive to changes of the SO₂ concentration than to changes of the OH concentration and the availability of SO₂ is the most important factor for new particle formation. At last, since the dilution ratio during advection was not well defined, effects of dilution were

investigated. If no dilution was taken into account, then the initial SO$_2$ was one tenth of the base case value. Consequently, nucleation and growth of particles were weaker but since dilution did not decrease number concentration the final N50 and N100 were around doubled. However, N200 was 36% lower and N300 was the same than in the base case. When the dilution ratio was 5 the most significant changes were observed in N50 and N100 which increased around 30% and in N300 which decreased by 34%.
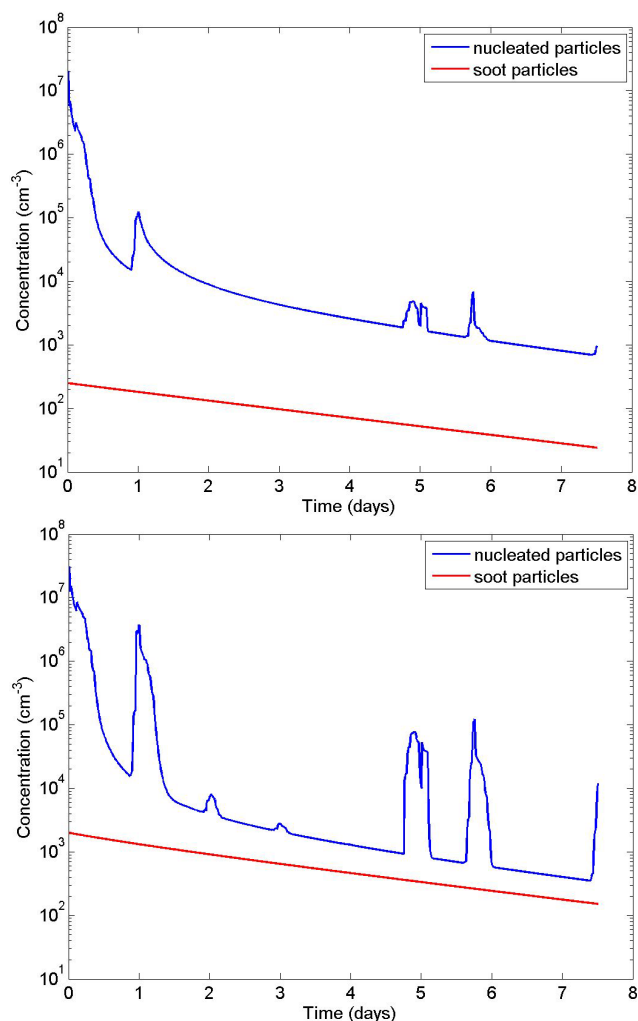
6 Soot particle coating

Next, we discuss the influence of the observed excess SO$_2$ on soot particles released by the same fossil fuel combustion sources which released the observed excess SO$_2$. Those fossil fuel combustion generated soot particles, initially present in the plume, which have escaped from cloud induced removal during the initial plume ascent, experienced coating by H$_2$SO$_4$/H$_2$O during the upper troposphere travel (26 April–3 May).

In order to estimate the coating of soot particles (soot particles with an H$_2$SO$_4$/H$_2$O coating are hereafter termed ternary particles) we have made simulations using the simplified model MONO32 (Pirjola et al., 2003).

The initial soot particle concentration (just after the initial ascent) may be estimated from the initial (just after the initial ascent) mass ratio for SO$_2$ and soot and the initial SO$_2$ concentration of 2.9×10^{11} cm^{-3} (as inferred from our measurements; see above). We have considered an initial (just after the initial ascent) SO$_2$/soot mass ratio of 16, which is typical for Chinese anthropogenic emissions (see above). Measurements in Asian pollution plumes over the East Pacific (Dunlea et al., 2008) obtained a mass ratio for sulfate and soot of about 15.5. Considering a plume age of say 4 days, and a mean SO$_2$ 1/e-lifetime of 10 days, the fraction of converted SO$_2$ would be about 33%. Hence, for an initial SO$_2$/soot mass ratio of 16 one would obtain a sulfate/soot mass ratio of about 16, which is similar to the SO$_4$/soot ratio measured in East Asian pollution plumes over the East Pacific. Assuming initial soot particles to have a diameter of 100 nm and a specific mass density of 2.0 g/cm^3, one obtains an initial (just after the initial ascent) soot particle number concentration of about 2000 cm^{-3}.

We have made soot coating simulations assuming an initial soot particle diameter of 100 nm (mono-modal distribution) and we have made simulations for different initial soot particle concentrations ranging from 250 to 2000 cm^{-3}. GSA uptake by soot was allowed to occur simultaneously to GSA conversion to binary (H$_2$SO$_4$/H$_2$O) particles. Ternary particles were allowed to coagulate with binary particles and with other ternary particles. Also self-coagulation between binary particles was taken into account.
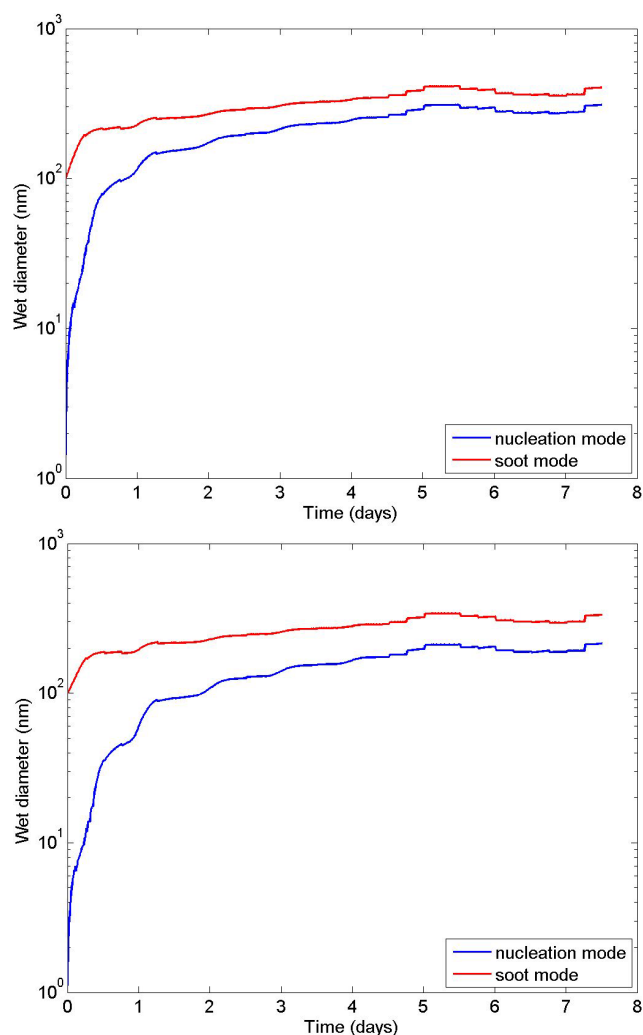
Figure 11 shows the model results for initial soot particle concentrations of 2000 cm^{-3} (lower panel) and 250 cm^{-3}

Fig. 11. Time sequence of the number concentrations of binary and ternary particles for initial soot particle concentrations of 2000 cm^{-3} (lower panel), and 250 cm^{-3} (upper panel).
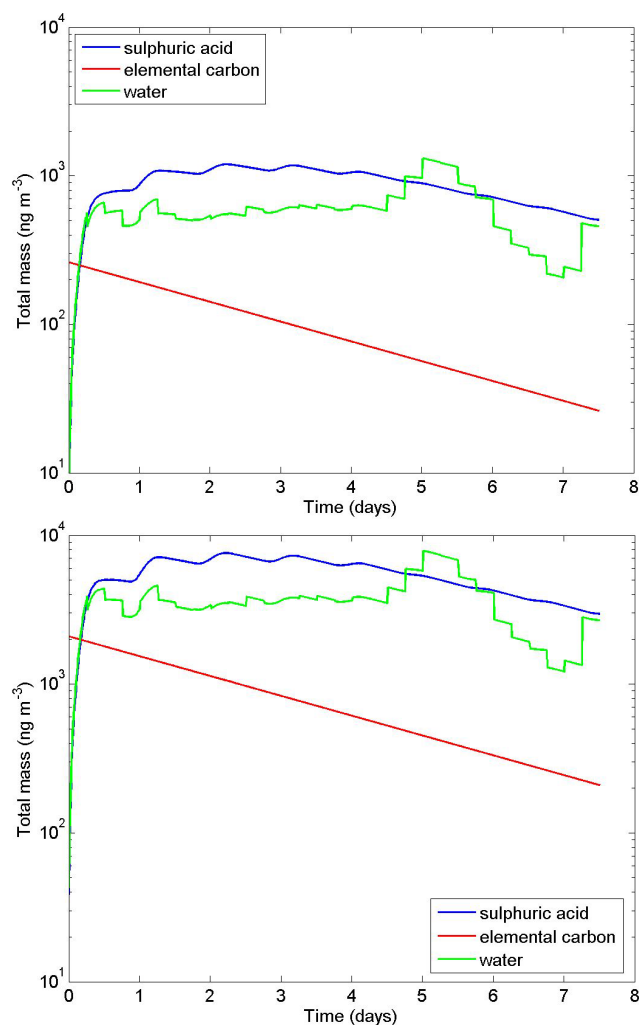
(upper panel). Plotted are time sequences of the number concentrations of binary and ternary particles. Ternary particles decrease exponentially from 2000 to 130 and from 250 to 24 cm^{-3}, respectively. The decrease is mostly due to plume dilution. The curves for binary particles have pronounced local maxima, due to new binary particle formation by nucleation.

Figure 12 shows time sequences of the wet diameters of ternary and binary particles for initial soot particle concentrations of 2000 cm^{-3} (lower panel) and 250 cm^{-3} (upper panel). Ternary particle diameters increase from 100 nm to 340 nm and 330 nm, respectively. Binary particle diameters increase to 220 nm and 250 nm, respectively. On 1 May, both curves have pronounced local maxima, due to additional hygroscopic size growth associated with the local maximum of RHW.

Fig. 12. Time sequence of the wet diameters of binary and ternary particles for initial soot particle concentrations of 2000 cm^{-3} (lower panel), and 250 cm^{-3} (upper panel).

Fig. 13. Time sequence of the total mass of each components of ternary H$_2$SO$_4$/H$_2$O/soot particles for initial soot particle concentrations of 2000 cm^{-3} (lower panel), and 250 cm^{-3} (upper panel).

Figure 13 shows time sequences of the soot mass, H$_2$SO$_4$ mass, and H$_2$O mass of ternary particles. On 26 April, shortly after the initial ascent, when GSA formation sets on, H$_2$SO$_4$ and H$_2$O contained in the ternary particles increase steeply while soot decreases due to plume dilution. On 27–28 April, sulfuric acid increases further, while H$_2$O remains nearly constant, and soot decreases further. On the following days, H$_2$SO$_4$ and soot continue to decrease. By contrast, H$_2$O exhibits pronounced local maxima (1 and 3 May), which are due to additional hygroscopic growth resulting from local maxima of RHW (see Fig. 7). During most of the upper troposphere travel of the plume parcel, the H$_2$SO$_4$ component makes the largest contribution to the total mass of ternary particles. Only on 1 May, when RHW was markedly elevated (up to 58%; see Fig. 7), the H$_2$O component makes the largest contribution.

7　Light scattering and absorption

Binary particles scatter but do not appreciably absorb sunlight. Ternary particles scatter and absorb sunlight and absorption is enhanced by the H$_2$SO$_4$/H$_2$O coating. On 1 May, when the plume parcel ascended to 7400 m altitude and when RHW reached a pronounced maximum the mean diameters of binary and ternary particles were largest (see Fig. 12). Therefore, light extinction by scattering should have been largest. The mean wet diameters of binary particles were about 210 and 240 nm for initial soot particle concentrations of 2000 and 250 cm^{-3}, respectively.

For example, for a wavelength of 550 nm and a particle refractive index of 1.5, the light scattering cross section increases steeply as the wet diameter of an H$_2$SO$_4$/H$_2$O particle increases to about 700 nm. Considering mean binary

particle diameters of 210 and 240 nm (on 1 May) and corresponding number concentrations of 740 and 1100 cm^{-3}, the light scattering coefficients are about 1.2×10^{-6} and 1.1×10^{-6} cm^{-1}. Hence, when neglecting light absorption, the practical visibility range (four 1/e lengths) becomes about 33 km. When considering in addition also light extinction by ternary particles, one obtains, for 1 May, practical visibility ranges of about 27 and 31 km, for initial soot particle concentrations of 2000 and 250 cm^{-3}, respectively. In comparison, in the absence of aerosol particles the practical visibility range dictated only by Rayleigh scattering of light (wavelength: 550 nm) by atmospheric gas molecules would be about 300 km at 7400 m altitude. Considering a horizontal dimension of the plume on 1 May of at least 500 km (see Fig. 4), the grown H$_2$SO$_4$/H$_2$O particles should have caused severe horizontal visibility degradation in the plume parcel.

Light absorption by a coated soot particle is larger than light absorption by an uncoated soot particle. The light absorbtion enhancement depends on the location of the soot particle (ranging from adhesion to the surface of a binary particle to concentric encapsulation), the thickness and the refractive index of the coating. For example for a soot particle diameter of 100 nm and concentric encapsulation, the light (wavelength 550 nm) absorption enhancement initially increases with increasing diameter of the ternary particle and remains nearly constant at about 3–4 for ternary particle diameters larger than about 500 nm (Fuller et al., 1999; Schnaiter et al., 2005). For a wavelength of 550 nm, the single scattering albedo (ratio of scattering cross section and extinction cross section) increases to about 0.8. This implies that about 20% of the light extinction induced by the ternary particles is due to absorption.

In the East Asian plume parcel ternary particles reach mean diameters of about 340 nm (Fig. 12). Therefore, the light absorption enhancement reaches nearly the maximum values of 3–4. Evidently, the SO$_2$ initially present in the plume parcel was sufficient to built up a massive H$_2$SO$_4$/H$_2$O coating of soot particles, which markedly altered their morphology and substantially increased the light absorption efficiency.

However, it is conceivable that soot particles present just after the ascent of 24/25 April, were not bare but had already a coating. If they had an H$_2$SO$_4$/H$_2$O coating already before the initial ascent, they were relatively hydrophilic which tends to increase the probability that they experienced removal by cloud processes. If they were bare or coated with organics, they probably would have been hydrophobic, which tends to increase their lifetime with respect to nucleation scavenging during the initial ascent.

8 Cloud condensation nuclei

The critical diameter of an H$_2$SO$_4$/H$_2$O aerosol particle required to allow the particle to act as a water vapor conden-
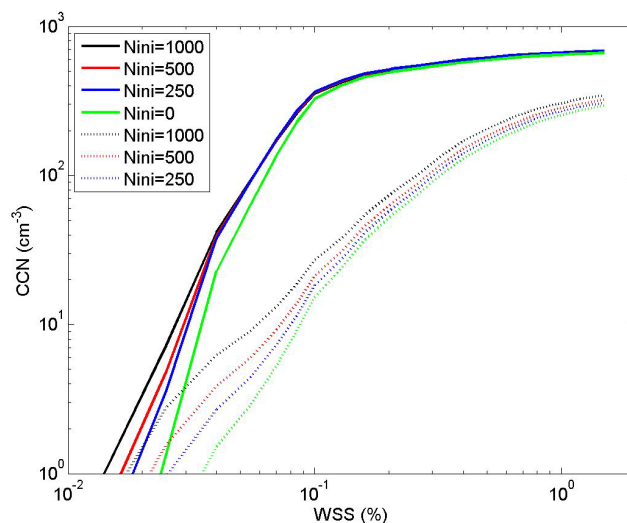
Fig. 14. Number concentration CCN of activated H$_2$SO$_4$/H$_2$O aerosol particles as function of the water vapor supersaturation WSS (for model runs A, B, C and D). Solid curves: with sulfuric acid formation. Dotted curves: without sulfuric acid formation.

sation nucleus decreases steeply with increasing water vapor supersaturation (WSS). For example, a H$_2$SO$_4$/H$_2$O particle with a wet diameter of 300 nm acts as a water vapor condensation nucleus already at a water vapor supersaturation of less than 0.1%.

Figure 14 shows, for the AEROFOR model runs A, B, C, and D , the final (3 May) number concentration CCN of activated H$_2$SO$_4$/H$_2$O aerosol particles as a function of the water vapor supersaturation WSS. Sulfuric acid formation was either operative (solid curves) or switched off (dashed curves). Without sulfuric acid formation, the four curves are similar and increase slowly with WSS. Although initial particle concentrations for runs A–D are much different the curves for runs A–D are very similar. This reflects the dominance of entrained particles, which are the same for runs A–D. Due to mixing with ambient air, ambient aerosol particles become permanently entrained into the diluting plume where they grow by coagulation. When sulfuric acid formation is switched on, new particles are formed in the plume and grow preferably by GSA condensation and to a smaller extend also by coagulation. Also, preexisting particles grow by GSA condensation.

When sulfuric acid formation is operative (solid curves), the four curves are nearly identical, but increase much more steeply and reach higher final values. The increase is steepest in the WSS range between about 0.07 and 0.1. In this range also the ratio of solid and dashed curves is largest. For example for WSS=0.1, this ratio is about 20. The large ratio indicates that concentrations of larger particles increase due to strong particle growth, counteracting plume dilution, which tends to strongly decrease particle concentrations.

Typical atmospheric WSS may reach up to about 2% (Pruppacher and Klett, 2000) and WSS of 0.1% can easily built up even in relatively weak updrafts. Therefore, according to our model simulations, the plume parcel intercepted by the Falcon on 3 May 2006 contained large concentrations of H$_2$SO$_4$/H$_2$O particles, which have the potential to become CCN already at WSS of only 0.1%. However, our meteorological analysis indicates that water vapor supersaturation with respect to liquid water did not occur in the air mass for the period of 26 April–3 May. The largest RHW of 58% occurred on 1 May during a temporary ascent, but no supersaturation (with respect to liquid water) occurred. Therefore, the grown aerosol particles could not become water vapor condensation nuclei during that period.

After 3 May, according to HYSPLIT forward simulations (Fig. 5 in the supplementary information: http://www.atmos-chem-phys.net/9/4729/2009/acp-9-4729-2009-supplement.zip), the plume traveled at high altitudes (mostly around 8000–9000 m) over the North Polar region and East Eurasia. During this additional 10-day upper troposphere travel, the plume is expected to have experienced further strong dilution (by a factor of about 5–10) and additional SO$_2$ conversion to GSA and additional aerosol growth by binary GSA condensation and coagulation. On 13–14 May, the plume descended rapidly and reached about 2000 m altitude over the West Pacific. At this height, only a relatively weak reascent of the plume would have been sufficient to activate the aged H$_2$SO$_4$/H$_2$O particles and let them act as cloud condensation nuclei. Due to the additional strong plume parcel dilution, the concentration of grown particles containing East Asian sulfur and soot (taken up by the air parcel on 24 April over central East Asia) is expected to be only about 40–80 cm^{-3}, which represents about 10–20% of the ambient free troposphere aerosol concentration (425 cm^{-3}; see above). However the aged particles, containing sulfur released from East Asian pollution sources, are much larger (mean diameter: larger than about 300–400 nm) than the above considered ambient background free troposphere particles (mean wet diameter at RHW=58%: 53 nm). Therefore, these larger aged particles have the potential to become CCN at significantly smaller WSS. Hence, even at a plume parcel age of about 20 days, the aged particles may still play a significant role as CCN.

9   Summary and conclusions

We have investigated the origin, evolution and impact of an East Asian SO$_2$ pollution plume, which was detected on 3 May 2006 at 5000–7000 m altitude over Europe by our airborne measurements. Our investigations, which involved model simulations of back-trajectories, plume dispersion, SO$_2$ conversion, and aerosol formation and growth, indicate that the observed excess SO$_2$ originated from central East Asia, most likely from fossil fuel combustion sources.

About 8–7 days prior to our measurements, the plume was ascending over central East Asia , probably in a cyclonic system and an associated warm conveyor belt, to an altitude of about 9000 m. Interestingly, during this ascent, a large fraction of the available SO$_2$ must have escaped from cloud induced scavenging. After the initial ascent, the plume descended slowly while it experienced advection across the North Pacific, North America, and the North Atlantic. On 3 May the plume extended from the Canary Islands, across the British Isles to Southern Norway and had a length of about 4000 km and measured 500 km across. During the 7.5 days of high altitude advection, clouds were absent inside and above but often were present below the plume. Hence clouds did not attenuate but rather increase solar UV-radiation in the plume. This allowed increased OH-formation and increased OH-induced SO$_2$ conversion to gas-phase sulfuric acid (GSA). Initially, this led to large GSA concentrations, which induced H$_2$SO$_4$/H$_2$O nucleation leading to numerous new H$_2$SO$_4$/H$_2$O aerosol particles. Binary H$_2$SO$_4$/H$_2$O condensation and particle coagulation led to particle growth. On day number 6 of the high altitude advection (1 May), about 40% of the H$_2$SO$_4$/H$_2$O particles in the plume had wet diameters larger than 340 nm, which caused severe horizontal visibility degradation. On 3 May, the day of our airborne measurements, about 50% of the particles had dry diameters larger than 200 nm and therefore had the potential to act as water vapor condensation nuclei in liquid cloud formation whenever water vapor supersaturations would exceed 0.4%. Soot particles, which may have survived the initial plume ascent would have become a component of internally mixed ternary (H$_2$SO$_4$/H$_2$O/soot) particles whose H$_2$SO$_4$/H$_2$O mass fraction, on 1 May, would have been about 98%. This would have dramatically altered the soot particle morphology (particle compaction) and would also have increased the light absorption cross section by a factor of about 2.3, compared to the geometric light absorption cross section of the bare soot particle. Forward trajectory simulations starting on 3 May (day of our measurements) suggest that the plume parcel continued its upper troposphere travel and passed over the North Polar region, East Eurasia, and hereafter on 13–14 May descended to about 2000 m altitude above the West Pacific. There, only a moderate reascent would have been sufficient to activate the aged aerosol particles to become CCN. Therefore it seems that the aged (about 20 days) particles may have played a significant role as CCN. The investigations of the plume should be extended in the future by an attempt to simulate the plume by using a global model.

References

Andreae, M., Jones, C., and Cox, P.: Strong present-day aerosol cooling implies a hot future, Nature, 435, 1187–1190, 2005.

Arnold, F., Schneider, J., Gollinger, K., Schlager, H., Schulte, P., Hagen, D., Whitefield, P., and van Velthoven, P.: Observation of upper tropospheric sulfur dioxide- and acetone-pollution: Potential implications for hydroxyl radical and aerosol formation, Geophys. Res. Let., 24, 57–60, 1997.

Barth, M.: Numerical modeling of sulfur and nitrogen chemistry in a narrow cold- frontal rainband: the impact of meteorological and chemical parameters, J. Appl. Meteorol., 33, 855–868, 1994.

Bethan, S., Vaughan, G., Gerbig, C., Volz-Thomas, A., Richer, H., and Tiddeman, D.: Chemical air mass differences near fronts, J. Geophys. Res., 103, 13413–13434, 1998.

Bey, I., Jacob, D., Logan, J., and Yantosca, R.: Asian chemical outflow to the Pacific in spring: Origins, pathways, and budgets, J. Geophys. Res., 106, 23097–23113, 2001.

Brock, C., Hudson, P., Lovejoy, E., Sullivan, A., Nowak, J., Huey, L., Cooper, O., Cziczo, D., de Gouw, J., Fehsenfeld, F., Holloway, J., Hübler, G., Lafleur, B., Murphy, D., Neuman, J., Nicks Jr., D., Orsini, D., Parrish, D., Ryerson, T., Tanner, D., Warneke, C., Weber, R., and Wilson, J.: Particle characteristics following cloud-modified transport from Asia to North America, J. Geophys. Res., 109, D23S26, doi:10.1029/2003JD004198, 2004.

Clegg, S. and Abbatt, J.: Uptake of Gas-Phase SO$_2$ and H$_2$O$_2$ by Ice Surfaces: Dependence on Partial Pressure, Temperature, and Surface Acidity, J. Phys. Chem. A, 105, 6630–6636, 2001.

Cooper, O., Forster, C., Parrish, D., Trainer, M., Dunlea, E., Ryerson, T., Hübler, G., Fehsenfeld, F., Nicks, D., Holloway, J., de Gouw, J., Warneke, C., Roberts, J., Flocke, F., and Moody, J.: A case study transpacific warm conveyor belt transport: Influence of merging airstreams on trace gas import to North America, J. Geophys. Res., 109, D23S08, doi:10.1029/2003JD003624, 2004.

Crutzen, P. and Lawrence, M.: The Impact of Precipitation Scavenging on the Transport of Trace Gases: A 3-Dimensional Model Sensitivity Study, J. Atmos. Chem., 37, 81–112, 2000.

de Reus, M., Krejci, R., Williams, J., Fischer, H., Scheele, R., and Ström, J.: Vertical and horizontal distributions of the aerosol number concentration and size distribution over the northern Indian Ocean, J. Geophys. Res., 106, 28629–28641, doi:2001JD900017, 2001.

Ding, A., Wang, T., Xue, L., Gao, J., Stohl, A., Lei, H., Jin, D., Ren, Y., Wang, X., Wei, X., Qi, Y., Liu, J., and Zhang, X.: Transport of north China air pollution by midlatitude cyclones: Case study of aircraft measurements in summer 2007, J. Geophys. Res., 114, D08304, doi:10.1029/2008JD011023, 2009.

Dunlea, E. J., DeCarlo, P. F., Aiken, A. C., Kimmel, J. R., Peltier, R. E., Weber, R. J., Tomlison, J., Collins, D. R., Shinozuka, Y., McNaughton, C. S., Howell, S. G., Clarke, A. D., Emmons, L. K., Apel, E. C., Pfister, G. G., van Donkelaar, A., Martin, R. V., Millet, D. B., Heald, C. L., and Jimenez, J. L.: Evolution of Asian aerosols during transpacific transport in INTEX-B, Atmos. Chem. Phys. Discuss., 8, 15375–15461, 2008, http://www.atmos-chem-phys-discuss.net/8/15375/2008/.

Fiedler, V., Dal Maso, M., Boy, M., Aufmhoff, H., Hoffmann, J., Schuck, T., Birmili, W., Hanke, M., Uecker, J., Arnold, F., and Kulmala, M.: The contribution of sulphuric acid to atmospheric particle formation and growth: a comparison between boundary layers in Northern and Central Europe, Atmos. Chem. Phys., 5, 1773–1785, 2005, http://www.atmos-chem-phys.net/5/1773/2005/.

Fiedler, V., Nau, R., Ludmann, S., Arnold, F., Schlager, H., and Stohl, A.: East Asian SO$_2$ pollution plume over Europe – Part 1: Airborne trace gas measurements and source identification by particle dispersion model simulations, Atmos. Chem. Phys., 9, 4717–4728, 2009, http://www.atmos-chem-phys.net/9/4717/2009/.

Finlayson-Pitts, B. J. and Pitts, J. N. J.: Chemistry of the upper and lower atmosphere, Academic Press, San Diego, London, first edn., 2000.

Fuchs, N.: The Mechanics of Aerosols., Pergamon Press, London, 1964.

Fuchs, N. and Sutugin, A.: Highly dispersed aerosol, Hidy, G. M. and Brock, J. R. (Eds): Topics in current aerosol research, Pergamon, New York, 1971.

Fuller, K., Malm, W. C., and Kreidenweis, S.: Effects of mixing on extinction by carbonaceous particles, J. Geophys. Res., 104, 15941–15954, doi:1998JD100069, 1999.

Garrett, T., Radke, L., and Hobbs, P.: Aerosol Effects on Cloud Emissivity and Surface Longwave Heating in the Arctic, J. Atmos. Sci., 59, 769–778, 2002.

Hanson, D. and Lovejoy, E.: Measurement of the Thermodynamics of the Hydrated Dimer and Trimer of Sulfuric Acid, J. Phys. Chem. A, 110, 9525–9528, doi:10.1021/jp062844w, 2006.

Harshvardhan, Schwarz, S., Benkovitz, C., and Guo, G.: Aerosol Influence on Cloud Microphysics Examined by Satellite Measurements and Chemical Transport Modelling, J. Atmos. Sci., 59, 714–725, 2002.

Huang, K., Zhuang, G., Xu, C., Wang, Y., and Tang, A.: The chemistry of the severe acidic precipitation in Shanghai, China, Atmos. Res., 89, 149–160, 2008.

IPCC: Intergovernmental Panel On Climate Change Report, IPCC, 2007.

Kolb, C., Jayne, J., Worsnop, D., Molina, M., Meads, R., and Viggiano, A.: Gas phase reaction of sulphur trioxide with water vapor, J. Am. Chem. Soc., 116, 10314–10315, 1994.

Kreidenweis, S., Zhang, Y., and Taylor, G.: The effects of clouds on aerosol and chemical species production and distribution 2. Chemistry model description and sensitivity analysis, J. Geophys. Res., 102, 23867–23882, 1997.

Laaksonen, A., Pirjola, L., Kulmala, M., Arnold, F., Raes, F., and Wohlfrom, K.-H.: Upper tropospheric SO2 conversion into sulfuric acid aerosols and cloud condensation nuclei, J. Geophys. Res., 105, 1459–1469, 2000.

Lee, S., Reeves, J., Wilson, J., Hunton, D., Viggiano, A., Miller, T.,

Ballenthin, J., and Lait, L.: Particle Formation by Ion Nucleation in the Upper Troposphere and Lower Stratosphere, Science, 301, 1886–1889, doi:10.1126/science.1087236, 2003.

Lee, S., Wilson, J., Baumgardner, D., Herman, R., Weinstock, E., LaFleur, B., Kok, G., Anderson, B., Lawson, P., Baker, B., Strawa, A., Pittman, J., Reeves, J., and Bui, T.: New particle formation observed in the tropical/subtropical cirrus clouds, J. Geophys. Res., 109, 20209, doi:10.1029/2004JD005033, 2004.

Lelieveld, J., Crutzen, P., Ramanathan, V., et al.: The Indian Ocean Experiment: Widespread Air Pollution from South and Southeast Asia, Science, 291, 1031, doi:10.1126/science.1057103, 2001.

Lesins, G., Chylek, P., and Lohmann, U.: A study of internal and external mixing scenarios and its effect on aerosol optical properties and direct radiative forcing, J. Geophys. Res., 107, 4094, doi:10.1029/2001JD000973, 2002.

Liu, K. and Chan, J.: Climatological Characteristics and Seasonal Forecasting of Tropical Cyclones Making Landfall along the South China Coast, Mon. Weather Rev., 131, 7210–7254, doi: 10.1175/2554.1, 2003.

Longo, B., Rossignol, A., and Green, J.: Cardiorespiratory health effects associated with sulphurous volcanic air pollution, Public Health, 122, 809–820, 2008.

Lovejoy, E., Hanson, D., and Huey, L.: Kinetics and products of the gas phase reaction of SO$_2$ with water, J. Phys. Chem., 100, 19911–19916, 1996.

Menon, S. and Saxena, V.: Role of sulfates in regional cloud-climate interactions, Atmos. Research, 47-48, 299–315, 1998.

Menzel, W., Frey, R., Zhang, H., Wylie, D., Moeller, C., Holz, R., Maddux, B., Baum, B., Strabala, K., and Gumley, L.: MODIS Global Cloud-Top Pressure and Amount Estimation: Algorithm Description and Results, J. Appl. Meteorol. Clim., 47, 1175–1198, doi:10.1175/2007JAMC1705.1, 2008.

Newell, R., Thouret, V., Cho, J., Stoller, P., Marenco, A., and Smit, H.: Ubiquity of quasi-horizontal layers in the troposphere, Nature, 398, 316–319, 1999.

Pirjola, L.: Effects of the increased UV radiation and biogenic VOC emissions on ultrafine aerosol formation, J. Aerosol Sci., 30, 355–367, 1999.

Pirjola, L. and Kulmala, M.: Development of particle size and composition distribution with a novel aerosol dynamics model, Tellus, 53B, 491–509, 2001.

Pirjola, L., Kulmala, M., Wilck, M., Bischoff, A., Stratmann, F., and Otto, E.: Formation of sulphuric acid aerosols and cloud condensation nuclei: An expression for significant nucleation and model comparison, J. Aerosol Sci,, 30, 1079–1094, 1999.

Pirjola, L., Tsyro, S., Tarrason, L., and Kulmala, M.: A monodisperse aerosol dynamics module – a promising candidate for use in the Eulerian long-range transport model, J. Geophys. Res., 108, 4258, doi:10.1029/2002JD002867, 2003.

Pruppacher, H. and Klett, J.: Microphysics of clouds and precipitation, Kluwer Academic Publishers, Dordrecht, The Netherlands, 2000.

Raes, F., Van Dingenen, R., Cuevas, E., Van Velthoven, P., and Prospero, J.: Observations of aerosols in the free troposphere and marine boundary layer of the subtropical Northeast Atlantic: Discussion of processes determining their size distribution, J. Geophys. Res., 102, 21315–21328, doi:97JD01122, 1997.

Ramanathan, V., Crutzen, P., Kiehl, J., and Rosenfeld, D.: Aerosol, climate, and the hydrological cycle, Science, 294, 2119–2124, 2001.

Reiner, T. and Arnold, F.: Laboratory flow reactor measurements of the reaction SO$_3$ + H$_2$O + M → H$_2$SO$_4$ + M: Implications for gaseous H$_2$SO$_4$ and aerosol formation in the plume of jet aircraft, Geophys. Res. Lett., 20, 2659–2662, 1993.

Reiner, T. and Arnold, F.: Laboratory investigations of gaseous sulfuric acid formation via SO$_3$ + H$_2$O + M → H$_2$SO$_4$ + M: Measurements of the rate constant and products identification, J. Chem. Phys., 101, 7399–7407, 1994.

Rodhe, H., Dentener, F., and Schulz, M.: The Global Distribution of Acidifying Wet Deposition, Environ. Sci. Technol., 36, 4382–4388, 2002.

Schnaiter, M., Linke, C., Möhler, O., Naumann, K., Saathoff, H., Wagner, R., Schurath, U., and Wehner, B.: Absorption amplification of black carbon internally mixed with secondary organic aerosol, J. Geophys. Res., 110, D19 204, doi:10.1029/2005JD006046, 2005.

Seinfeld, J. and Pandis, S.: Atmospheric Chemistry and Physics, John Wiley & Sons, Inc., first edn., 1998.

Seinfeld, J. and Pandis, S.: Atmospheric Chemistry and Physics, John Wiley & Sons, Inc., second edn., 2006.

Singh, H. B., Brune, W. H., Crawford, J. H., Flocke, F., and Jacob, D. J.: Chemistry and transport of pollution over the Gulf of Mexico and the Pacific: spring 2006 INTEX-B campaign overview and first results, Atmos. Chem. Phys., 9, 2301–2318, 2009, http://www.atmos-chem-phys.net/9/2301/2009/.

Stockwell, W. and Calvert, J.: The Mechanism of the HO-SO$_2$ reaction, Atmos. Environ., 17, 2231–2235, 1983.

Stohl, A., Eckhardt, S., Forster, C., James, P., Spichtinger, N., and Seibert, P.: A replacement for simple back trajectory calculations in the interpretation of atmospheric trace substance measurements, Atmos. Environ., 36, 4635–4648, 2002.

Stohl, A., Forster, C., Frank, A., Seibert, P., and Wotawa, G.: Technical note: The Lagrangian particle dispersion model FLEXPART version 6.2, Atmos. Chem. Phys., 5, 2461–2474, 2005, http://www.atmos-chem-phys.net/5/2461/2005/.

Streets, D. and Waldhoff, S.: Present and future emissions of air pollutants in China: SO$_2$, NO$_x$, and CO, Atmos. Environ., 34, 363–374, 2000.

Sunyer, J., Atkinson, R., Ballester, F., Le Tertre, A., Ayres, J., Forastiere, F., Forsberg, B., Vonk, J., Bisanti, L., Anderson, R., Schwartz, J., and Katsouyanni, K.: Respiratory effects of sulphur dioxide: a hierarchical multicity analysis in the APHEA 2 study, Occupational and Environmental Medicine, 60, doi:10.1136/oem.60.8.e2, 2003.

Thornton, D., Bandy, A., and Blomquist, B.: Transport of sulfur dioxide from the Asian Pacific Rim to the North Pacific troposphere, J. Geophys. Res., 102, 28489–28499, 1997.

Vehkamäki, H., Kulmala, M., Napari, I., Lehtinen, K., Timmreck, C., Noppel, M., and Laaksonen, A.: An improved parameterization for sulfuric acid – water nucleation rates for tropospheric and stratospheric conditions, J. Geophys. Res., 107, 4622–4631, doi:10.1029/2002JD002184, 2002.

Venners, S., Wang, B., Xu, Z., Schlatter, Y., Wang, L., and Xu, X.: Particulate matter, sulfur dioxide, and daily mortality in Chongqing, China, Environ. Health Perspect., 111, 562–567, 2003.

Wernli, H. and Davies, H.: A Lagrangian-based analysis of extratropical cyclones. I: The method and some applications, Q. J. Roy.

Meteorol. Soc., 123, 467–489, 1997.

Xiong, X., Chiang, K., Sun, J., Barnes, W., Guenther, B., and Salomonson, V.: NASA EOS Terra and Aqua MODIS on-orbit performance, Adv. Space Res., 43, 413–422, doi:10.1016/j.asr.2008.04.008, 2009.

Zhang, Q., Streets, D. G., Carmichael, G. R., He, K., Huo, H., Kannari, A., Klimont, Z., Park, I., Reddy, S., Fu, J. S., Chen, D., Duan, L., Lei, Y., Wang, L., and Yao, Z.: Asian emissions in 2006 for the NASA INTEX-B mission, Atmos. Chem. Phys. Discuss., 9, 4081–4139, 2009,
http://www.atmos-chem-phys-discuss.net/9/4081/2009/.

Zhang, R., Khalizov, A., Pagels, J., Zhang, D., Xue, H., and McMurry, P.: Variability in morphology, hygroscopicity, and optical properties of soot aerosols during atmospheric processing, Proceedings of the National Academy of Sciences, 105, 10291–10296, 2008.